LETTERS

Non-volcanic tremor and low-frequency earthquake swarms

David R. Shelly[1], Gregory C. Beroza[1] & Satoshi Ide[2]

Non-volcanic tremor is a weak, extended duration seismic signal observed episodically on some major faults, often in conjunction with slow slip events[1–4]. Such tremor may hold the key to understanding fundamental processes at the deep roots of faults, and could signal times of accelerated slip and hence increased seismic hazard. The mechanism underlying the generation of tremor and its relationship to aseismic slip are, however, as yet unresolved. Here we demonstrate that tremor beneath Shikoku, Japan, can be explained as a swarm of small, low-frequency earthquakes, each of which occurs as shear faulting on the subduction-zone plate interface. This suggests that tremor and slow slip are different manifestations of a single process.

Tremor is difficult to locate because it lacks the distinct impulsive, body wave arrivals used by traditional earthquake location methods; but occasionally tremor in Japan contains relatively energetic and isolated pulses that have been identified as low-frequency earthquakes (LFEs) by the Japan Meteorological Agency[5]. Compared with nearby ordinary earthquakes, LFEs are enriched in low frequencies (~1–5 Hz) and depleted at higher frequencies. Precise relocations of LFEs beneath western Shikoku reveal that they lie along the dipping subduction interface at depths of 30–35 km (ref. 6). On the basis of their locations and the character of their waveforms, LFEs were inferred to represent fluid-enabled shear slip on the plate boundary as part of concurrently observed slow slip events[6], rather than fluid flow as previously proposed[5].

To test this interpretation further, Ide *et al.* calculated the mechanism of LFEs using two independent methods that exploit waveform similarity between LFEs and regular earthquakes in the subducting slab: analysis of LFE P-wave first motions and an empirical moment tensor inversion of LFE S waves[7]. As shown in Fig. 1, these techniques each yield results consistent with the mechanisms of slow slip events as well as the most recent megathrust earthquake in this area. All these lines of evidence indicate that LFEs are generated by shear slip on the plate interface. Does a similar mechanism generate continuous tremor?

If the same shear-faulting source generates both LFEs and tremor, we might expect to see additional weaker events within tremor with waveforms similar to the previously identified LFEs[6]. The spectrum of tremor tracks that of LFEs, but with slightly smaller amplitude (Fig. 2), which supports the possibility of a common physical mechanism for the two phenomena.

To test this hypothesis, we used the waveforms of 677 of the best-recorded LFEs in this region as 'template events' in a matched-filter technique to search tremor waveforms systematically for portions of the tremor that strongly resemble one or more template LFEs[8]. We require each template event to be recorded at a minimum of six three-component stations. Correlation coefficients from these stations/components are then stacked to produce an 'array' correlation sum. We record a detection when this correlation sum peaks above a threshold value.

As a detected event must possess the same pattern of waveforms across multiple stations and components as the template event, their locations must closely coincide. An example of a positive detection is shown in Fig. 3, which plots the correlation sum as a function of time, as well as waveforms and cross-correlation coefficients at the time of detection across the network. Additional examples of detections and non-detections are shown in Supplementary Fig. S1. Because we are working with complex waveforms with low signal-to-noise ratios, individual channels of data show relatively weak correlations and contain insufficient power to detect events when examined in isolation. The strength of the matched-filter approach comes from simultaneously considering waveforms across the network, which increases the detection power dramatically.

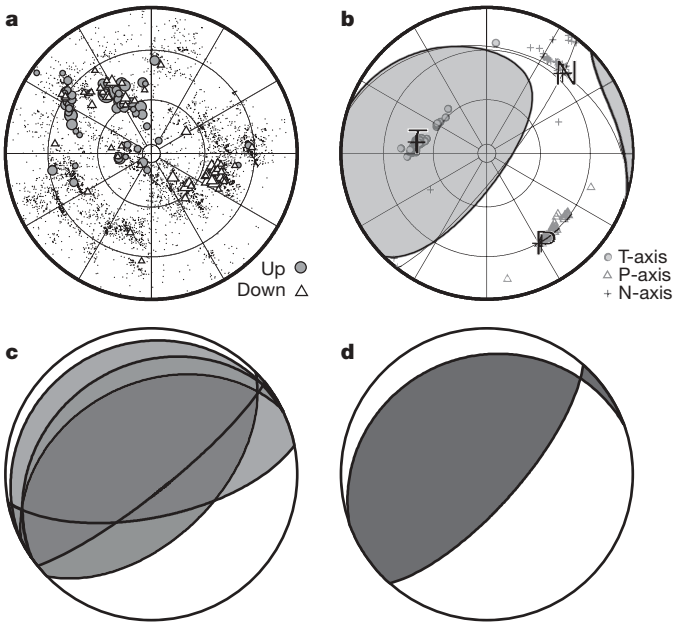

Figure 1 | Comparison of LFE, slow slip event, and megathrust earthquake mechanisms. **a**, P-wave first motions determined by Ide *et al.* for low frequency earthquakes by cross-correlation-based first motion determination[7]. Filled circles and open triangles indicate compressional (up) and dilatational (down) first motions for LFE P waves, respectively. The signal-to-noise ratio for most observations (small dots) is too low to determine the polarity. **b**, Moment tensor inversion results from empirical Green's function analysis of LFE S waves. Tension (T), pressure (P) and null (N) axes are shown together with symbols showing uncertainty and corresponding P-wave first motion distribution. **c**, Overlay of the mechanism for three slow slip events near the study area[15]. **d**, Mechanism of the 1946 Nankai earthquake[16], which is the most recent megathrust earthquake in this region and representative of relative plate motion between the Philippine Sea plate and the over-riding plate on the dipping plate interface of the Nankai trough subduction zone. All are shown in equal area projection of the lower focal hemisphere.

[1]Department of Geophysics, 397 Panama Mall, Stanford University, Stanford, California 94305-2215, USA. [2]Department of Earth and Planetary Science, University of Tokyo, Hongo 7-3-1, Bunkyo-ku, Tokyo 113-0033, Japan.

The ability to extract a weak signal from noisy data is demonstrated by the synthetic example discussed in the Supplementary Methods and shown in Supplementary Fig. S2. We use the correlation sum as our detection statistic, and register a 'strong' detection when a value of 8 times the median absolute deviation is exceeded. For a normally distributed random variable, this corresponds to an exceedence probability of $\sim 3.3 \times 10^{-8}$. On the basis of synthetic tests such as the example shown in Supplementary Fig. S2, we estimate a location uncertainty for 'strong' detections of approximately 3 km.

In order to allow for the possibility that tremor is excited in the vicinity of, but not at exactly the same location as, an LFE in our catalogue, we also allow for 'weak' detections. In this case, we take the maximum correlation coefficient from a 0.4-s window at each station before summing. For the weak detection, the threshold is set at 9 times the median absolute deviation of the distribution of correlation sums plus the median of this distribution, which corresponds to a probability of $\sim 6.4 \times 10^{-10}$, for the gaussian case.

Our detection technique reveals a nearly continuous sequence of LFEs during periods of active tremor. Statistical considerations argue against random detections, but perhaps an even more compelling argument can be made on the basis of the highly clustered nature of the positive detections. The detection statistic that we use is normalized, which means that it does not depend on absolute amplitudes. Therefore, there is nothing in the construction of the measurement to favour positive detections of one LFE over another if the tremor consists of incoherently radiated energy or noise. Thus, we expect that false positive detections should be geographically random.

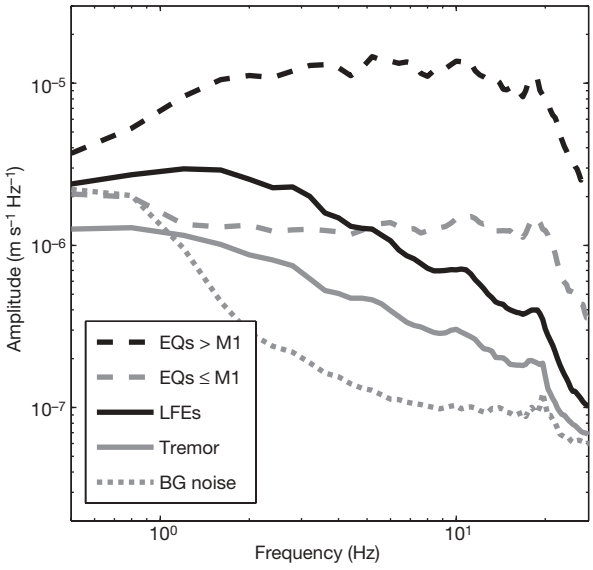

Figure 2 | Comparison of earthquake/LFE/tremor spectra. Shown is a comparison of stacked, uncorrected spectral amplitude from Hi-net velocity seismograms (horizontal components) from multiple nearby events of various kinds. LFEs and regular earthquakes (EQs) are selected from the same hypocentral region (33.4–33.6 °N, 132.6–132.8 °E, depths 25–45 km). Tremor is selected from approximately the same region. For LFEs and regular earthquakes, spectra are calculated for S-wave arrivals for a 2.5-s window, from 0.5 s before to 2.0 s after the catalogue phase arrival. Background (BG) noise is calculated from a 2.5-s window, 2 s before to 0.5 s after the origin time of regular earthquakes. Tremor spectra are calculated from sequential 2.5-s windows over a 400-s time period. Earthquakes are separated by magnitude. We do not divide LFEs by size because their magnitude determination method changed during our study period. In this example, we use: 43 earthquakes with magnitude $M > 1$, 52 earthquakes with $M \leq 1$, and 233 LFEs. LFE (solid black line) and tremor (solid grey line) spectra are highly similar, but tremor has smaller amplitude. Small earthquake (dashed black) and very small (dashed grey) earthquake spectra are highly similar to each other, but lack the rapid decay of amplitude with increasing frequency that is characteristic of both tremor and LFE spectra.

Figure 4 shows that rather than being random, the distribution of positive detections is highly clustered. Not only are the detections spatially coherent during a tremor burst, they also show an interesting time progression. Figure 4 demonstrates the detailed evolution of two 30-min episodes of active tremor on different portions of the plate interface. The second example (Fig. 4b) is notable in that it shows an episode of tremor migration, with the source moving approximately 15 km up-dip along the interface in just over 20 min. This is not a unique occurrence—similar episodes are observed at other times and sometimes propagate in the opposite direction. This along-dip migration rate of $\sim 45\,\mathrm{km\,h^{-1}}$ is much faster than along-strike migration rates of $5–17\,\mathrm{km\,d^{-1}}$ previously reported in this region[1] and in Cacadia[9,10]. Although these slower rates may still govern the longer-term average migration, with the matched-filter technique we can resolve more complex behaviour and faster migration rates along both strike and dip. Notably, we also find instances when multiple tremor sources, separated by up to ~20 km, are active simultaneously. This may explain some of the variation, particularly in depth, found in previous estimates of tremor location in Cascadia[10,11]. A detailed look at tremor behaviour during the periods shown in Fig. 4 is available in the Supplementary Movies.

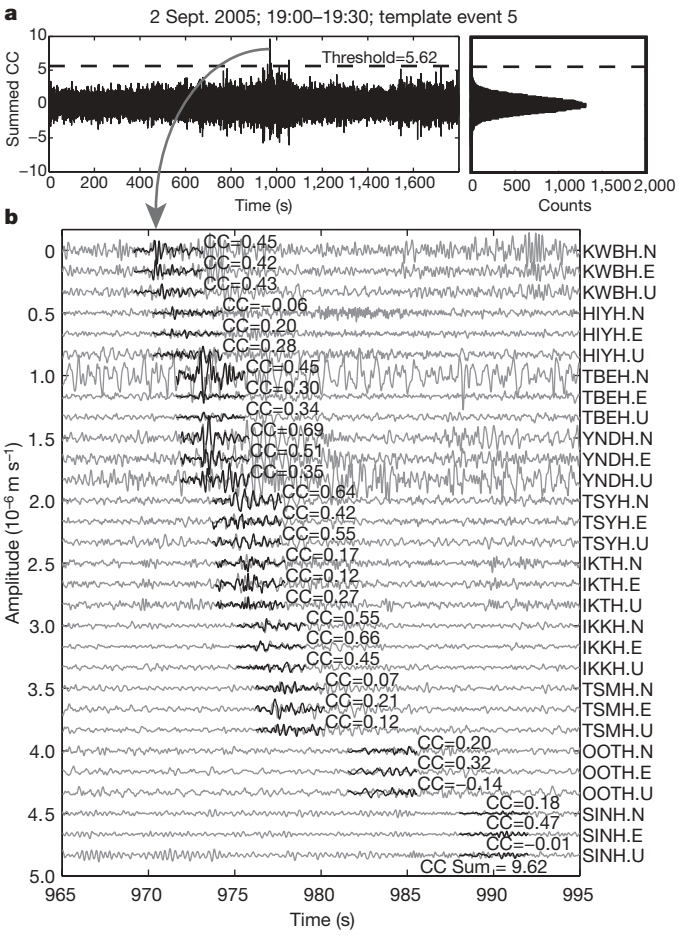

Figure 3 | Example of a detected LFE. a, Correlation sum function for template event 5 during the same 30-min period as highlighted in Fig. 4b. CC, correlation coefficient. A histogram of correlation sum values is shown on the right. **b**, Continuous tremor waveforms are shown in grey and template event waveforms in black for each component of 10 Hi-net stations. The CC for each trace is shown next to the template event waveforms. Station names and components are given to the right of each trace. Additional detections (not shown) are also present during this time window. Waveforms are bandpass filtered between 1 and 8 Hz and template event amplitudes are scaled to match the continuous data. Although individual cross correlation coefficients are modest, they are overwhelmingly positive and extremely unlikely to have occurred by chance.

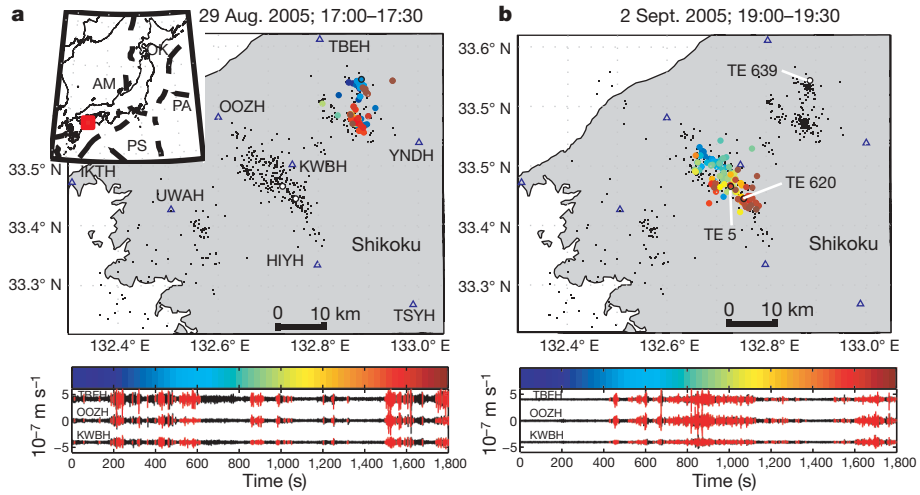

Figure 4 | Detection of LFE swarms forming tremor. a, Top panel; map view of westernmost Shikoku, showing areas active (coloured circles) during the 30-min period on 29 August 2005 beginning at 17:00, colour coded with time (see colour scale below). Only 'strong' detections are shown. Note the clear spatial coherence of detected events with time. The spatial distribution of positive detections is not built into the detection algorithm, but emerges from the data. Black dots show epicentral locations of template LFEs used in this study. The depth of these events corresponds to the plate interface at 30–35 km (ref. 6). Blue triangles denote station locations. Bottom panel shows east-component waveforms at three Hi-net stations, bandpass filtered between 1 and 8 Hz. Portions plotted in red indicate times with a detected event ('strong' or 'weak') similar to a template event. Inset, the regional tectonics, with the red box indicating the area shown in the main panel. PA, Pacific plate; PS, Philippine Sea plate; AM, Amur plate; OK, Okhotsk plate. **b**, Same as **a**, but beginning 2 September 2005 at 19:00. In this episode, a clear up-dip migration of the tremor source can be seen. The locations of template events (TE) referred to in Fig. 3 and Supplementary Fig. S1 are also labelled.

The dense coverage of LFE template sources in the region active in Fig. 4b allows us to attribute the tremor source almost entirely to the sources of known LFEs. This is illustrated by the waveforms shown in Fig. 4b, where portions explained by LFEs are plotted in red. In this case, the match between detected LFEs and tremor is nearly perfect. In the example of Fig. 4a, previously recorded LFEs still explain the vast majority of the tremor, but occasionally weak tremor occurs without LFE detections. This probably reflects the main limitation of our technique—the uneven distribution of our LFE template sources. As we only have template LFEs in places that, at least occasionally, rupture energetically enough to produce an identifiable phase across many stations, some areas of the fault may generate weak tremor without producing 'template-strength' LFEs. In these instances, tremor may be generated too far from a template event to register as a positive detection, even though it may be occurring as a weak LFE. The relatively sparse coverage of the region active in Fig. 4a by template LFE events supports this interpretation.

The heterogeneous distribution of LFEs (Fig. 4) probably reflects properties of the plate boundary. Clusters of relatively strong LFEs may occur in places of geometric or compositional variations where the fault sticks and slips as part of much larger scale slow slip transients—a process analogous to that proposed for some foreshock sequences[12] or earthquake swarms[13,14] in other environments. In this case, high fluid pressure on the plate boundary could allow slip to occur under low shear stress, resulting in relatively slow rupture and slip velocities (compared with ordinary earthquakes) and a corresponding deficit in high frequency energy (Fig. 2).

Using previously recorded and located LFEs as template events, we have established that tremor in Shikoku can be regarded as a swarm of LFEs and thus is generated by a series of small shear slip events on the plate boundary. Our approach allows us to track the source of tremor with unprecedented temporal and spatial resolution, and hence may provide similar precision in monitoring slow slip. It is important to watch such behaviour carefully, as slow slip transients can load adjacent locked portions of a fault and increase the probability of large, damaging earthquakes.

Received 12 October 2006; accepted 6 February 2007.

1. Obara, K. Nonvolcanic deep tremor associated with subduction in southwest Japan. *Science* **296,** 1679–1681 (2002).
2. Rogers, G. & Dragert, H. Episodic tremor and slip on the Cascadia subduction zone: The chatter of silent slip. *Science* **300,** 1942–1943 (2003).
3. Nadeau, R. M. & Dolenc, D. Nonvolcanic tremors deep beneath the San Andreas fault. *Science* **307,** 389 (2005); published online 9 December 2004 (doi:10.1126/science.1107142).
4. Obara, K., Hirose, H., Yamamizu, F. & Kasahara, K. Episodic slow slip events accompanied by non-volcanic tremors in southwest Japan subduction zone. *Geophys. Res. Lett.* **31,** doi:10.1029/2004GL020848 (2004).
5. Katsumata, A. & Kamaya, N. Low-frequency continuous tremor around the Moho discontinuity away from volcanoes in the southwest Japan. *Geophys. Res. Lett.* **30,** doi:10.1029/2002GL015981 (2003).
6. Shelly, D. R., Beroza, G. C., Ide, S. & Nakamula, S. Low-frequency earthquakes in Shikoku, Japan and their relationship to episodic tremor and slip. *Nature* **442,** 188–191 (2006).
7. Ide, S., Shelly, D. R. & Beroza, G. C. Mechanism of deep low frequency earthquakes: further evidence that deep non-volcanic tremor is generated by shear slip on the plate interface. *Geophys. Res. Lett.* **34,** doi:10.1029/2006GL028890 (2007).
8. Gibbons, S. J. & Ringdal, F. The detection of low magnitude seismic events using array-based waveform correlation. *Geophys. J. Int.* **165,** 149–166 (2006).
9. Dragert, H., Wang, K. & Rogers, G. Geodetic and seismic signatures of episodic tremor and slip in the northern Cascadia subduction zone. *Earth Planets Space* **56,** 1143–1150 (2004).
10. Kao, H. *et al.* Spatial-temporal patterns of seismic tremors in northern Cascadia. *J. Geophys. Res.* **111,** doi:10.1029/2005JB003727 (2006).
11. Kao, H. *et al.* A wide depth distribution of seismic tremors along the northern Cascadia margin. *Nature* **436,** 841–844 (2005).
12. Dodge, D. A., Beroza, G. C. & Ellsworth, W. L. Detailed observations of California foreshock sequences: implications for the earthquake initiation process. *J. Geophys. Res.* **101,** 22371–22392 (1996).
13. McGuire, J. J., Boettcher, M. S. & Jordan, T. H. Foreshock sequences and short-term earthquake predictability on East Pacific Rise transform faults. *Nature* **434,** 457–461 (2005).
14. Vidale, J. E. & Shearer, P. M. A survey of 71 earthquake bursts across southern California: Exploring the role of pore fluid pressure fluctuations. *J. Geophys. Res.* **111,** doi:10.1029/2005JB004034 (2006).
15. Hirose, H. & Obara, K. Repeating short- and long-term slow slip events with deep tremor activity, around the Bungo channel region, southwest Japan. *Earth Planets Space* **57,** 961–972 (2005).
16. Ando, M. A fault model of the 1946 Nankaido earthquake derived from tsunami data. *Phys. Earth Planet. Int.* **28,** 320–336 (1982).

Supplementary Information is linked to the online version of the paper at www.nature.com/nature.

Acknowledgements This material is based upon work supported by the National Science Foundation. We thank S. Nakamula for assistance with the Hi-net data. All data were obtained from the NIED Hi-net data server.

Author Information Reprints and permissions information is available at www.nature.com/reprints. The authors declare no competing financial interests. Correspondence and requests for materials should be addressed to D.R.S. (dshelly@pangea.stanford.edu).